Journal of Engineering and Technological Advances (JETA)
https://jeta.segi.edu.my/index.php/segi
2025 Vol. 10 No. 2

NANOEMULSION BASED ON PEPPERMINT ESSENTIAL OIL AS A CARRIER FOR ZINC OXIDE NANOPARTICLES: SYNTHESIS AND CHARACTERIZATION

[1]Dzulkharnien N.S.F., [1]Jaais, M.A.D., [1]Kofli, N.T., [1]Othman, A.R., [3,4] Noor Akhmazillah Mohd Fauzi, [3,4] Angzzas Sari Mohd Kassim, [3,4] Sity Aishah Mansur, [1,2*] Rohani, R.

[1] Department of Chemical and Process Engineering, Faculty of Engineering & Built Environment, Universiti Kebangsaan Malaysia, 43600, UKM Bangi, Selangor, Malaysia.

[2] Research Centre for Sustainable Process Technology, Faculty of Engineering & Built Environment, Universiti Kebangsaan Malaysia, 43600, UKM Bangi, Selangor, Malaysia.

[3] Department of Chemical Engineering Technology, Faculty of Engineering Technology, Universiti Tun Hussein Onn Malaysia, 86400, Johor, Malaysia.

[4] ProNature Living Solutions Sdn. Bhd., Universiti Tun Hussein Onn Malaysia, 86400, Johor, Malaysia.

* Corresponding Author: rosiah@ukm.edu.my Tel.: (+60)-38921 6977

Received: 24 October 2025; Accepted: 11 November 2025; Published: 31 December 2025
doi: 10.35934/segi.v10i2.158

Highlights:

- The optimum conditions were at 7.8 ml of Tween 80, 1 ml of SLS and 2 ml of distilled water.
- Low storage temperature had increased the viscosity of the NE and improved the stability of NE.
- The slow-release behaviour of ZnO/PO-NE had reduced the antibacterial efficacy.

Abstract: This study investigated the synthesis and characterization of peppermint essential oil-based nanoemulsions (PO-NE) incorporated with zinc oxide nanoparticles (ZnO NPs) for improving the antibacterial applications, in a way to address the global challenges of antibiotic resistance issues. Nanoemulsions (NE) offered a promising strategy to enhance ZnO NP stability and targeted delivery. In this study, the synthesis parameters of PO-NE incorporated ZnO NO were optimized, by manipulating the surfactant and water ratios using the Response Surface Methodology (RSM) and One-Factor-At-a-Time (OFAT) approaches. Fourier transform infrared spectroscopy (FTIR) was used to validate the functional groups in the molecular structure, while particle size, polydispersity index (PDI), and zeta potential were determined by using dynamic light scattering (DLS). The thermal property of the optimized ZnO/PO-NE was evaluated using differential scanning calorimetry (DSC), alongside the stability and antibacterial activity against *Escherichia coli* (*E. coli)* and *Staphylococcus aureus* (*S. aureus)*. It was found that the optimized ZnO/PO-NE exhibited small particle sizes (280.633

This is an open-access article under the CC BY-NC-ND license

± 14.791 nm), a moderate PDI (0.537 ± 0.102), a high zeta potential (-17.100 ± 0.700 mV), and possessed an enhanced thermal stability. The antibacterial activity (6.3 ± 0.0 mm against *E. coli*, 6.0 ± 0.0 mm against *S. aureus*) suggested a controlled release behaviour, which has a high potential for further development. This work significantly contributes to SDG 3, promoting Good Health and Well-being.

Keywords: peppermint oil; nanoemulsion; zinc oxide; antibacterial; response surface methodology

1. Introduction

Nanoparticles (NPs) typically defined as materials ranging from 1 to 100 nanometers (nm) in size, with unique properties such as antibacterial, optical, magnetic, catalytic and electronic properties. Furthermore, NPs possess advanced characteristics such as biocompatibility, anti-inflammatory, and antibacterial properties, effective drug delivery, bioavailability, tumour targeting, and bio-absorption, leading to growth in biotechnology and microbiological applications (Mansoori and Soelaiman, 2005). Exploration of NPs are foreseen to be potential in wide sectors, including environmental, biomedical, and food industry such as water waste treatment, environmental monitoring, functional food additives, and antimicrobial agents (Bayda *et al.*, 2019).

NE is a type of NPs that defines as heterogeneous mixtures of two immiscible liquids, such as water and oil, stabilized with surfactants or emulsifying agents. Their size ranges from 10 to 1000 nm. There are several types of NE based on the dispersed and continuous phases, including oil-in-water (O/W) NE, water-in-oil (W/O) NE, and bi-continuous NE where both phases are continuous (Jaiswal, Dudhe and P K Sharma, 2014). O/W NE is dispersed in a continuous aqueous phase and is widely used in pharmaceutical, cosmetic, and food industries due to its ability to enhance the solubility and bioavailability of hydrophobic compounds. On the other hand, W/O NE is dispersed in a continuous oil phase and is promising for encapsulating hydrophilic compounds. NE can be produced through high-energy methods namely homogenization, ultrasonication or microfluidization, which uses an external energy to break down large droplets into nano-sized particles, and low-energy methods (Chuo and Setapar, 2022). The methods include spontaneous emulsification, phase inversion temperature (PIT), composition phase inversion (PIC) and others. Zinc oxide nanoparticles (ZnO NPs) are metal oxide nanoparticles exhibit excellent optical properties and good antibacterial agent. Nonetheless, their dose-dependent toxicity and poor solubility had hindered their usage for antibacterial agent applications (Abdelmigid *et al.*, 2022). Hence, recent research explores the

combination of nanoparticles of ZnO with NE systems, offering a promising strategy to enhance dispersibility and antibacterial efficacy. NE can carry NPs in a stable colloidal form, facilitating better interaction with bacterial cells and enhancing antimicrobial action. Of all NE, peppermint essential oil is a potential nanoemulsion because its antimicrobial properties, therapeutic effectiveness, pleasant aroma, and compatibility with various formulations that make it an optimal choice for producing oil-in-water nanoemulsions. This essential oil not only enhances the stability and efficacy of the formulation but also aligns with consumer demand for natural and effective products across various industries.

Therefore, in this study, an optimized NE system made up from peppermint essential oil (PO-NE) was developed, which incorporated with ZnO NPs by varying the volume of Tween 80, sodium lauryl sulphate (SLS) and distilled water, using two different optimization techniques, RSM and OFAT. The intrinsic properties of the optimized ZnO/PO-NE were verified using FTIR, DLS and DSC, while antibacterial property of the NE was studied using disc diffusion technique.

2. Materials and Methods

2.1. Materials

In this study, the peppermint essential oil was purchased from Personal Formula Resources (M) Sdn. Bhd, a local company based in Malaysia. Tween 80 and SLS were sourced from R&M Chemicals, while zinc acetate dihydrate was procured from Sigma Aldrich. The remaining chemicals such as sodium hydroxide (NaOH) and hydrochloric acid (HCl) were obtained from Thermo Fisher Scientific. *S. aureus* and *E. coli* strains were acquired from the American Type Culture Collection (USA) and stored at −20 °C in a Chill-500 single-door refrigerator. Muller Hinton Agar and Muller Hinton Broth (MHB) were obtained from Oxoid, UK. Commercial nanosized ZnO, with particle sizes < 50 nm and purity > 97%, was obtained from Sigma-Aldrich.

2.2. Methods

2.2.1. Preparation of ZnO NPs

ZnO NPs were prepared following the method reported in Dzulkharnien *et al.*, 2024. Briefly, 100 mL of 0.1 M zinc acetate and 5 mL of 20% v/v aloe vera peel extract were mixed for 1 hour, then 50 ml of 0.6 M NaOH solution was added into the clear solution until pH reached 13 and continued to mix for 2 hours. The mixture was then sonicated using an ultrasonicator

(Qsonica, USA) for 2 hours at 30˚C. After that, the mixture was centrifuged at 4500 rpm using a centrifuge (Sigma 2-16P Microcentrifuge) and then dried in an oven for 48 hours at 60˚C.

2.2.2. Synthesis of PO-NE using OFAT and RSM

Synthesis of PO-NE was conducted by adding certain volume of Tween 80, SLS and water and mixed thoroughly for 30 minutes. Two approaches, OFAT and RSM, were used to compare and finalize optimize synthesis condition of PO-NE. **Table 1** and **Table 2** show the experimental runs generated using OFAT and RSM-Box Behnken, respectively.

Table 1. Experimental run varying factor A, B and C using OFAT.

Run	Factor 1 A: Tween 80 (ml)	Factor 2 B: SLS (ml)	Factor 3 C: Water (ml)	Peppermint essential oil (ml)
A	7.8	0.5	2.0	8.0
B	8.3	0.5	2.0	8.0
C	8.8	0.5	2.0	8.0
D	8.3	0.0	2.0	8.0
E	8.3	0.5	2.0	8.0
F	8.3	1.0	2.0	8.0
G	8.3	0.5	1.5	8.0
H	8.3	0.5	2.0	8.0
I	8.3	0.5	2.5	8.0

Table 2. Independent variables with code levels in the design and responses involved in the optimization process

Independent variable	Unit	Symbol	Code level		
			-1	**0**	**+1**
Tween 80 volume	ml	A	7.8	8.3	8.8
SLS volume	ml	B	0.0	0.5	1.0
Water volume	ml	C	1.5	2.0	2.5
Response				**Unit**	**Symbol**
PDI				mW/Mn	R1
Particle size				nm	R2

2.2.3. Preparation of PO-NE Incorporated ZnO NPs

Once the optimized condition to synthesize PO-NE was decided, 7.8 ml of Tween 80 was dissolved in distilled water with 2 ml of 1% w/w ZnO NPs until a uniform solution was

obtained. Subsequently, 1 ml of SLS and 8 ml of PO was slowly added to the solution and mixed at a speed of 500 rpm at 25°C ± 1°C for 30 minutes.

2.2.4. Stability Test

Stability test was conducted through two methods, accelerated and centrifugation method. For the accelerated stability test, the NE was placed in a clean glass vial, and stored for 2 weeks at 4°C and 60°C. On every 0, 1, 3, 5, 7, 10, and 14 days, samples are taken where the appearance are evaluated. The sample was then observed and the appearance of the NE was assessed.

2.2.5. Antibacterial Study

E. coli and *S. aureus* bacteria that have been cultured in MHB solution were placed on agar plates by streaking method. The ZnO/PO-NE was dissolved in HCl and diluted to concentration of 100 mg/ml. 200 µL of the dissolved NE was placed on a disc and then placed on an agar plate containing bacterial streaks. The agar plate was then incubated at 37°C for 24 hours. A clear circle known as the zone of inhibition (ZOI) was measured using a ruler (15 cm long).

2.2.6. Characterization

FTIR (Thermo Fischer Scientific, US) was used to identify characteristic peaks related to functional groups and chemical bonds present on the surface of ZnO NPs and in the NE matrix. DSC (DSC 214 Polyma, NETZSCH) is used to measure the amount of heat energy absorbed or released by a sample when it undergoes a physical or chemical change such as phase transition (melting, crystallization, glass transition), chemical reaction, or thermal denaturation. DLS (Zetasizer Nano) was used to determine particle size, PI and zeta potential of NE.

3. Results and Discussion

3.1. Nanoemulsion Formulation of PO Using the OFAT and RSM Method

Table 3 and **Table 4** tabulated the findings from experimental run using OFAT and RSM-BBD design, respectively, by manipulated the volume of Tween 80, SLS and water. The PDI and particle size were assessed for each of conditions. Results from the study showed that moderate amounts of Tween 80 and distilled water created favorable conditions for the formation of stable NE, while the addition of SLS enhanced this stability through better emulsification. A careful balance between these formulation components is essential to achieve the desired properties of mint essential oil NE. These results underscore that formulation must consider the volume of individual ingredients and their interactions to optimize product performance (Milinčić *et al.*, 2024). According to the optimized output from both approaches, synthesis

condition with volume of Tween 80 = 7.8 ml, volume of SLS = 1 ml and volume of water = 2 ml, with consistent volume of PO (8 ml), that give result of 0.27 of PDI and 344.6 nm of size of particle.

Table 3. Experimental run using OFAT

Run	Factor 1 A: Tween 80 (ml)	Factor 2 B: SLS (ml)	Factor 3 C: Water (ml)	Peppermint essential oil (ml)	R1 PDI	R2 Particle size (nm)
A	7.8	0.5	2.0	8.0	0.26	381.7
B	8.3	0.5	2.0	8.0	0.33	377.2
C	8.8	0.5	2.0	8.0	0.39	545.7
D	8.3	0.0	2.0	8.0	0.37	398.9
E	8.3	0.5	2.0	8.0	0.32	367.2
F	8.3	1.0	2.0	8.0	0.27	344.6
G	8.3	0.5	1.5	8.0	0.39	384.7
H	8.3	0.5	2.0	8.0	0.32	367.2
I	8.3	0.5	2.5	8.0	0.44	427.9

Table 4. Response results of the Box-Behnken design with 17 runs.

Run	Factor 1 A: Tween 80 (ml)	Factor 2 B: SLS (ml)	Factor 3 C: Distilled water (ml)	Response R1: PDI	Response R2: Particle size (nm)
1	8.3	0.0	1.5	0.56	1096.7
2	8.3	0.5	2.0	0.37	394.9
3	8.3	1.0	2.5	0.24	526.3
4	8.3	1.0	1.5	0.49	540.6
5	8.8	1.0	2.0	0.35	395.5
6	8.3	0.5	2.0	0.32	367.2
7	8.3	0.0	2.5	0.37	422.03
8	7.8	0.5	2.5	0.26	381.7
9	7.8	1.0	2.0	0.27	344.6
10	8.8	0.0	2.0	0.39	545.7
11	8.8	0.5	1.5	0.37	535.9
12	7.8	0.0	2.0	0.35	476.7
13	8.8	0.5	2.5	0.44	427.9
14	8.3	0.5	2.0	0.37	439.8
15	8.3	0.5	2.0	0.40	384.7

16	8.3	0.5	2.0	0.61	722.6
17	7.8	0.5	1.5	0.88	2087.3

Table 5 shows the ANOVA results of the PDI model and particle size. A p-value in the ANOVA that lower than 0.05 indicates that the model is significant (Amirabedi, Yegani and Hesaraki, 2017). According to **Table 5**, p-value of PDI model is lower than 0.05 showing that the model is significant. In contrast, p-value for particle size models is slightly higher than 0.05, which indicates that the model is less significant. In this analysis, both models show that factor C and AC are significant factors, involving the independent variables of volume of Tween 80 and volume of distilled water.

Table 5. ANOVA results for the PDI and particle size model.

Source	**PDI**		**Particle size (nm)**	
	F-value	**P-value**	**F-value**	**P-value**
Model	3.48	0.0400	2.91	0.0654
A	0.4700	0.5099	2.28	0.1619
B	0.9800	0.3450	0.6409	0.4420
C	9.82	0.0106	7.45	0.0212
AB	0.0200	0.8913	0.0008	0.9781
AC	9.53	0.0115	6.07	0.0335
BC	0.0600	0.8140	1.04	0.3325
Residual				
Total Corr				

From the output from RSM-BBD, the final equation of the independent variable factors can be formulated, as shown in equation (1) and (2).

$$R1 = +0.4140 - 0.0270A - 0.0392B - 0.1238C + 0.0078AB + 0.1725AC - 0.0135BC \quad (1)$$

$$R2 = +593.55 - 173.15A - 91.77B - 312.83\,C - 4.56AB + 399.40\,AC - 165.09\,BC \quad (2)$$

where R1 is the PDI; R2 is the particle size; A, B, and C represent the volume of Tween 80, the volume of SLS and the value of water, respectively.

3.2. RSM-BBD surface response analysis

The 3D plot generated from the RSM-BBD illustrates how changes in certain parameters affect the desired response. The peaks and troughs on the surface indicate the region of optimal parameter combinations, where maximum efficiency and effectiveness are achieved. Based on the output from the models in **Table 5**, the relationship between the volume of Tween 80 (A) and distilled water(C), shows significant impact on PDI and particle size. **Figure 2** depicted the 3D plot of the response of PDI (R1) and particle size (R2) to changes in the volume of Tween 80 and distilled water. **Figure 2**(a) shows the area ranging from color coded blue (lower PDI values) to yellow (higher PDI values) and shows interaction between the volume of Tween 80 and volume of distilled water influence PDI. The red dots scattered above and below the surface represent the study values obtained for specific combinations of Tween 80 and water volume. Most of the study points align closely with the surface, indicating a good fit between the study data and the RSM-BBD model predictions. Similarly, **Figure 2**(b) illustrates a non-linear relationship where particle size decreases with increasing Tween 80 concentration at the optimum water volume. This visualization highlights that although surfactant concentration plays an important role in controlling particle size, maximizing one component without balancing it with the others is not sufficient to achieve the desired NE characteristics.

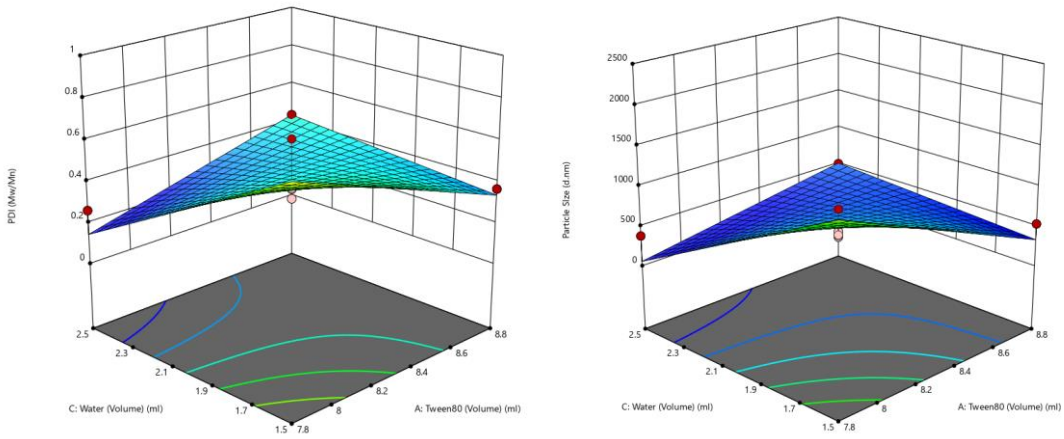

(**a**) (**b**)

Figure 2. 3D plot of the response: (**a**) PDI and (**b**) Particle size, to the volume change of Tween 80 and distilled water.

In conclusion, the 3D plot response surface analysis in RSM-BBD offers significant insights into how formulation factors interact to influence the performance of PO-NE. These findings highlight the importance of balancing surfactant concentration and aqueous phase content to minimize PDI and particle size while enhancing stability and efficacy. The flexibility and

predictive power of the RSM model, combined with the detailed visualization of interaction dynamics, supports its use as an important tool in the development and optimization of NE systems across a variety of fields.

3.3. Characterization of Physicochemical and Thermal Properties of ZnO/PO-NE

Particle Size, PDI and Zeta Potential

Particle size and PDI are important in determining the stability, quality, homogeneity and dispersibility of NE. Particle size plays an important role in understanding the physical properties, stability, and performance of NE. Small particle size (<200nm) indicates increased stability, while increasing particle size indicate instability and aggregation (Alhaddad *et al.*, 2024). PDI refers to the uniformity of particle size distribution in a NE, where the value range starts from 0 to 1. PDI <0.2 indicates small size distribution and uniform particles, making the formulation more stable. Zeta potential is a measure of the surface charge of NPs and is also an indicator of colloidal stability in NE suspensions. A high absolute value (± 30mV) suggests strong repulsion between particles, indicating good stability. A low value suggests a tendency for particles to reassemble, becoming less stable (Somala, Laosinwattana and Teerarak, 2022). In this study, particle size and its distribution were determined using DLS instrument. **Table 6** shows the particle size and PDI values of the formed NE. The results of comparing the particle size and PDI of PO-NE with and without ZnO NPs from the selected formulations obtained from the RSM results. **Table 6** shows the outcomes of particle size, PDI and zeta potential values of optimized PO-NE and ZnO/PO-NE.

Table 6. Particle size and PDI of PO-NE with and without ZnO NPs

Sample	Particle size (nm)	PDI	Zeta potential (mV)
PO-NE	295.000 ± 30.720	0.440 ± 0.012	-0.051 ± 0.019
ZnO/PO-NE	280.633 ± 14.791	0.537 ± 0.102	-17.100 ± 0.700

From **Table 6**, PO-NE and ZnO/PO-NE exhibited particle sizes below 300 nm, which were generally associated with an improved in the bioavailability and stability. This was particularly beneficial for the absorption and delivery of active compounds. Studies have reported that NE with smaller size particles showed a better dispersion and penetration abilities compared to the larger particles. Particle sizes around 296 nm were associated with enhanced antimicrobial activity in a study using *Nigella sativa* NE (Mutlu, 2024). Similarly, formulations exhibiting smaller average sizes have shown an increase in efficacy of the bioactive compounds, which is

important in ensuring that the active ingredient is effectively delivered to the target site in the biological systems.

Concurrently, PO-NE and ZnO/PO-NE demonstrated moderate PDI values, which is 0.440 and 0.530, respectively. Although the values are non-ideal, but they are still acceptable in most formulations. Studies suggest that such PDI values may indicate a moderate particle size distribution and can still be used in practical applications, albeit with some impact on stability (Thepwatee, Pinket and Rangauthok, 2024). For example, one study reported a PDI of 0.569±0.2 in a formulation using *Nigella sativa* NE, still showing promising results even though it exceeds the general value (0.1-0.2) (Mutlu, 2024). This suggests that although PDI suggests a wider dispersion, the stability of NE can still be maintained if other formulation parameters are well controlled.

The addition of ZnO NPs into NE was observed had reduced the particle size of the NE but increased the PDI value. This could be due to the stabilizing effect of ZnO NPs between the oil and water surfaces. The presence of these nanoparticles reduces the tendency of the emulsion particles to coalesce, driven by interparticle attraction (Kampa *et al.*, 2022). When ZnO NPs were evenly dispersed throughout the emulsion, they helped in maintaining a uniform and smaller particle size, promoting stability (Hunter *et al.*, 2024). As a result, this stability led to smaller particle sizes, beneficial in applications such as drug delivery (Kaur *et al.*, 2024). At the same time, an increase in the PDI value may be attributed to several factors, including aggregation of ZnO NPs in the emulsion and uneven distribution of surfactants (Cadena *et al.*, 2022). Higher PDI indicated a broader particle size distribution, arising from interactions between nanoparticles and between water and oil surfaces. These interactions allow for variations in the packing density of emulsion particles, which can lead to the formation of larger aggregates, thus increasing the PDI value (Kampa *et al.*, 2022).

According to **Table 6**, it can be observed that the zeta potential value of the PO-NE is -0.051 ± 0.019 mV while the zeta potential value of ZnO/PO-NE is -17.100 ± 0.700 mV. When comparing these two values, there was an increase in the zeta potential value of NE after adding ZnO NPs. The addition of ZnO NPs was observed to alter the surface charge characteristics of PO-NE. When ZnO NPs were incorporated into the formulation, due to their size and surface charge properties, they contributed positively to the overall zeta potential, leading to an improved stability through enhanced electrostatic repulsion among the particles. The increase in zeta potential may be attributed to the ionization of surface hydroxyl groups on ZnO NPs which may enhance their interaction with the aqueous phase. This enhanced zeta potential

reflects a shift towards a more stable emulsion system. Higher zeta potential led to an increase in the bioavailability and efficacy of peppermint oil, as demonstrated by enhanced release profiles under simulated physiological conditions (Zhu *et al.*, 2019; Omar *et al.*, 2023). Zeta potential influenced the encapsulation of the bioactive molecules between the oil-water interface, which in turn influenced the bioavailability of the essential oils.

3.4. Fourier Transform Infrared (FTIR) Analysis

FTIR analysis is an important technique used to characterize the chemical composition and interactions in PO-NE and the effect of incorporating ZnO NPs in it. **Figure 3** shows the FTIR spectra of the PO-NE and ZnO/PO-NE, while **Table 7** summarized the functional groups presence. The peaks at specific wave numbers indicated different bonds, which the peaks for ZnO NPs were typically around 400-600 cm^{-1}, O-H around 3400 cm^{-1}, C-O, and C-H stretching at 1093, 1457 and 2922 cm^{-1}, respectively (Kalaba *et al.*, 2024). In overall, the FTIR analysis showed that the interactions between the ZnO NPs and the PO have slightly modified the characteristic profile of the NE.

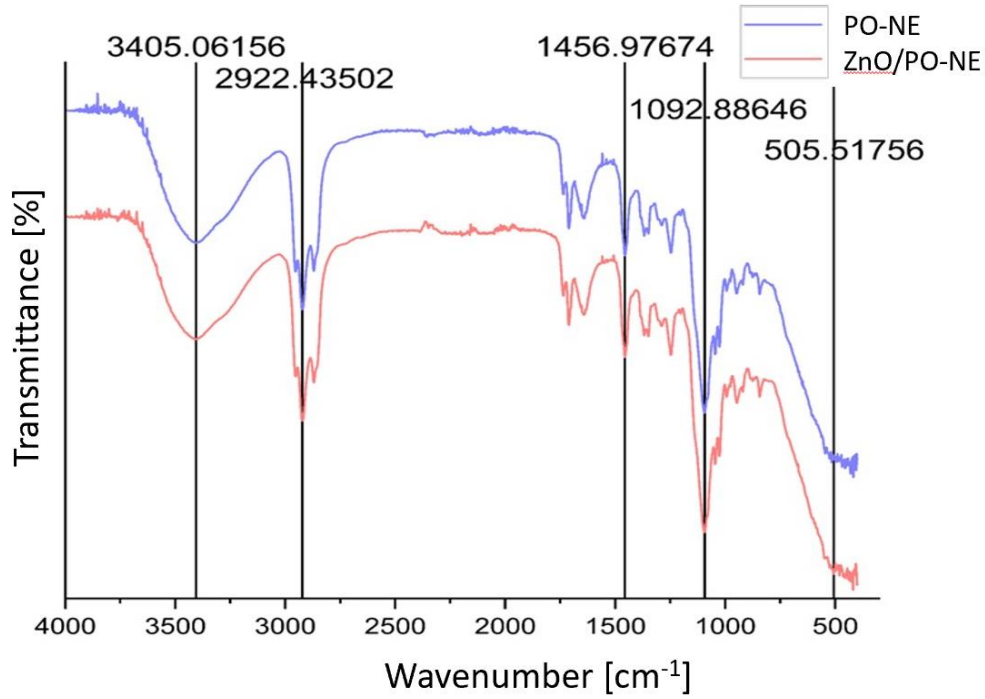

Figure 3. FTIR spectra of the PO-NE and ZnO/PO-NE

Table 7. Functional group for FTIR spectra and its data interpretation.

Wavenumber (cm^{-1})	Functional Group
3405	O–H stretching

2922	C–H stretching
1457	C–H bending
1093	C–O stretching
505	Zn–O stretching

3.5. Differential Scanning Calorimetry (DSC) Analysis

DSC analysis is an analytical technique used to investigate the thermal properties of PO-NE, both with and without ZnO NPs. **Figure 4** shows the DSC analysis graph of the formed NE. From **Figure 4**, it can be observed that PO-NE was more pronounced to endothermic peak at lower temperatures (below 100°C), suggested a greater heat absorption due to the volatile evaporation or possible melting of the components. In contrast, the ZnO/PO-NE sample exhibited a lower magnitude in its endothermic response across the same temperature range. This reduced in the heat absorption indicated that the addition of ZnO increased the thermal stability of the NE, likely by preventing the volatilization or decomposition of the PO components (Motelica *et al.*, 2023). Moreover, after reaching the minimum of their respective peaks, both curves have gradually returned to a less negative heat flow direction with increasing temperature, but the PO-NE sample has continued to display more negative values than the ZnO/PO-NE. This indicated that PO-NE underwent further heat loss at higher temperatures, while ZnO/PO-NE remained more stable (Bakeshlou *et al.*, 2024). In summary, the inclusion of ZnO in the PO-NE increased its resistance to thermal degradation, as indicated by the less pronounced endothermic peak. This greater thermal stability can be beneficial for extending the shelf life and improving the thermal performance of the product of PO-NE based in various applications.

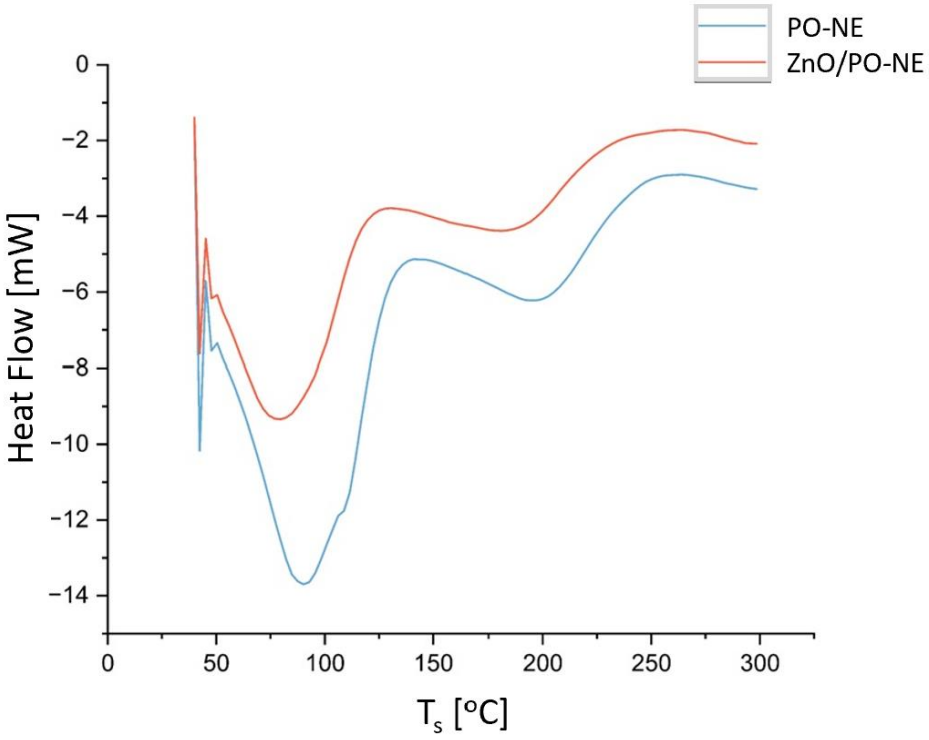

Figure 4. DSC analysis graph of PO-NE and ZnO/PO-NE

3.6. Stability of ZnO/PO-NE

Accelerated stability testing of NE at different temperatures, specifically at 4°C and 60°C, provided important insights into their physicochemical properties and long-term viability. This test investigated how the stability of NE changed over a period of 14 days when stored at these two temperatures. **Figure 5** shows the appearance of ZnO/PO-NE at 4°C and 60°C on days 0, 1, 3, 5, 7, 10 and 14.

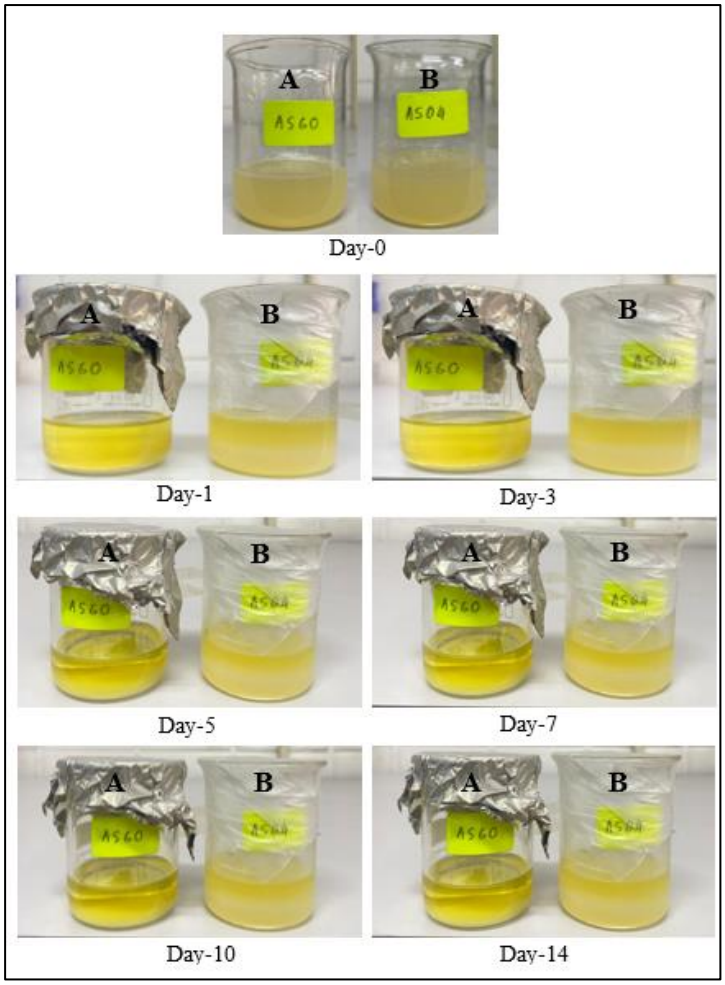

Figure 5. Visual of ZnO/PO-NE stored at A) 60°C and B) 4°C on days 0, 1, 3, 5, 7, 10, and 14.

From **Figure 5**, the state of the NE can be observed after storage at extreme temperatures. For the NE stored at 60°C, it can be observed that the transparency of the upper part of the NE increased, and there was a layer at the bottom of the beaker where ZnO NPs appeared to be deposited. The state of the NE over 14 days did not show any significant difference after the first day. For the NE stored at 4°C, it can be observed that the NE formed two layers, where the lower layer appeared cloudy and milky white. The state of the NE over 14 days also did not show any significant change, like the NE stored at 60°C. The presence of ZnO NPs in NE stored at 60°C showed the phenomenon of sedimentation, that closely related to several physicochemical factors involved in emulsion stability. One of the main causes of sedimentation was influenced by the storage temperature. As the temperature increased, the viscosity of the system decreased, which resulted in easier particle movement. In this case, increased temperature also caused aggregation of the ZnO NPs, which created a decrease in emulsion stability (Lima *et al.*, 2024). In contrast, at a lower applied temperature (4°C), the

viscosity of the system increased and this caused a decrease in the speed of movement of surfactant molecules, followed by instability of the emulsion layer (Adjonu *et al.*, 2022).This instability between the emulsion layers might also cause by a decrease in the electrostatic repulsion between the particles resulting from the decomposition or reduction in the amount of surfactant that may actively interact at the oil-water interface (Saberi, Fang and McClements, 2014). The continuity between oil and water particles became weaker at low temperatures, which could support the formation of the two layers in the mixture (Teng *et al.*, 2020).

3.7. Antibacterial Properties Study of ZnO/PO-NE

The antibacterial properties of ZnO/PO-NE has been evaluated using the disc diffusion method, which is a widely accepted technique in microbiology. **Table 8** shows the diameter of the ZOI using PO-NE and ZnO/PO-NE against the bacterial strains *E. coli* and *S. aureus* and the diagrams of the ZOI are shown in **Figure 6**.

Table 8. ZOI using PO-NE and ZnO/PO-NE on selected bacterial strains

Sample	ZOI (mm)		Source
	E. coli	***S. aureus***	
PO-NE	8.3 ± 1.5	10.0 ± 3.5	This study
ZnO/PO-NE	6.3 ± 0.6	6.0 ± 0.0	This study
Negative control (Distilled water)	0.0 ± 0.0	0.0 ± 0.0	This study
Positive control (Commercial ZnO NPs)	7.7 ± 0.9	11.0 ± 0.0	Dzulkharnien et al., 2024

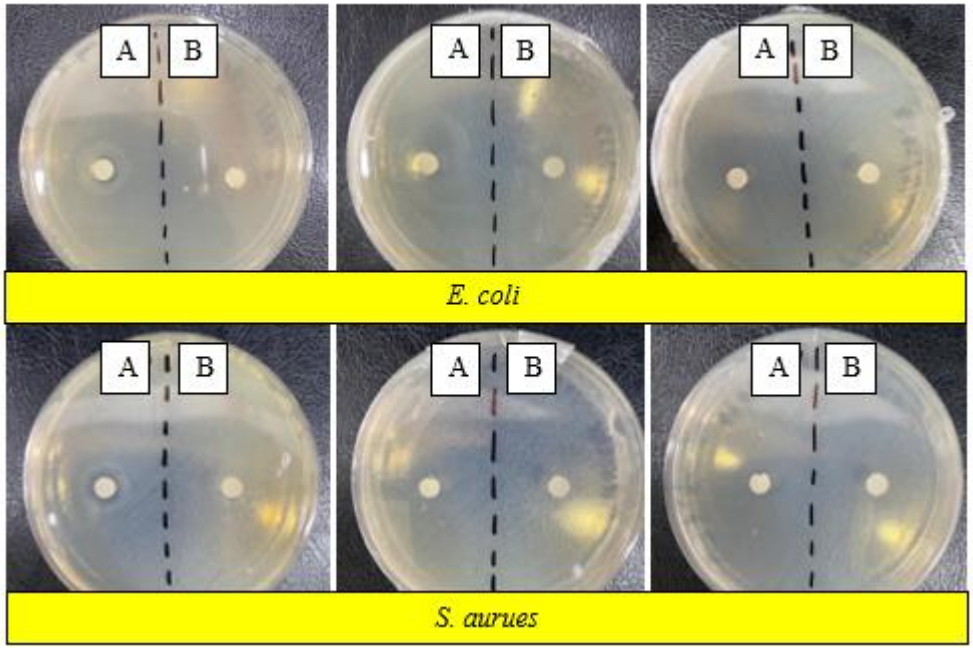

Figure 6. Diagram of ZOI using A) PO-NE and B) ZnO/PO-NE on *E. coli* and *S. aureus*

From **Table 8**, the antibacterial properties of the ZnO/PO-NE were observed and analyzed through the ZOI, which is the area where bacterial growth stops. The positive control using ZnO NPs alone, findings from the study by Dzulkharnien *et al.* (2024), showed a ZOI of 7.7 ± 0.9 mm and 11.0 ± 0.0 mm, underlining the beneficial aspects of ZnO NPs in displaying antibacterial activity on its own, on both the selected bacterial strains. For the *E. coli* bacterial strain, the PO-NE produced a ZOI of 8.3 ± 1.5 mm, meanwhile the ZOI for PO-NE sample against *S. aureus* exhibited a larger ZOI of 10.0 ± 3.5 mm, indicating stronger antibacterial activity compared to its performance against *E. coli*. Notably, the introduction of ZnO NPs resulted in a decrease in efficacy, with a ZOI of 6.3 ± 0.6 mm and 6.0 ± 0.0 mm on *S. aureus* and *E. coli*, respectively. This reduction suggested that although ZnO NPs contribute some antibacterial properties, they may also compete with the antimicrobial effect of PO or interfere with the overall antibacterial mechanism of the NE (Liu *et al.*, 2021). In addition, studies have found that when essential oils were used in a NE, their release rates can vary due to several factors. One important aspect is that NE provides a protective environment for essential oil compounds, such as menthol and menthone, which are the main active ingredients of PO (Kung *et al.*, 2014). This encapsulation can increase stability and prolong the delivery of these compounds. However, the slow-release properties can result in a reduction in the immediate concentration of antibacterial agents in the surrounding medium, which directly reflected in the size of the ZOI observed in the disc diffusion test (Zhang *et al.*, 2022).

4. Limitation and Recommendation

In general, although nanoemulsification aimed to enhance the delivery of bioactive compounds through enhanced dispersibility and surface area, it remained important to optimize the formulation in a way that maintained or enhanced antibacterial potency while compensating for the slow-release characteristics of ZnO NPs. Therefore, a few possible interactions between components, including the structural integrity of the NE and the release mechanism, are essentially needed to develop formulations that can maximize antibacterial efficacy without bringing up the drawbacks presented by the slow-release properties associated with the incorporation of ZnO NPs. There are include: (i) Oil Phase - Surfactant Interaction, (ii) ZnO NPs - Surfactant/Co-surfactant Interaction, (iii) ZnO NPs - Oil Phase Interaction, (iv) PO – ZnO NPs Interaction, (v) Aqueous Phase - NPs/Surfactant Interaction. These interactions could be balanced in a way to maintain NE stability, achieve controlled release of ZnO and maximize antibacterial activity without excessive delay in release due to the slow-release effect of ZnO.

5. Conclusion

This study was found to be successful in achieving its objectives by effectively optimizing the synthesis parameters of NE using OFAT and RSM study designs. The findings especially showed the interaction of the variables such as Tween 80 and SLS volumes. An optimized ZnO/PO-NE was successfully synthesized with a small particle size (280.633 ± 14.791 nm), a moderate PDI (0.537 ± 0.102), and a moderate zeta potential (-17.100 ± 0.700 mV), which was supported by FTIR and DSC analyses showing improved thermal stability and shelf life. However, sedimentation did occur during accelerated stability testing. The ZnO/PO-NE showed a less antibacterial efficiency compared to *E. coli* (6.3.0 ± 0.0 mm) and *S. aureus* (6.0 ± 0.0 mm), compared to independent components of NE. This finding however suggested that nanoemulsion might have controlled release properties and further optimization is needed.

Acknowledgement

The authors would like to thank Universiti Kebangsaan Malaysia for funding under Prototype Development Research Grant [PRGS/1/2024/TK05/UKM/02/1].

Credit Author Statement

Conceptualization, N.S.F.D. and M.A.D.J.; methodology, N.S.F.D., M.A.D.J., N.T.K, A.R.O.; software, M.A.D.J.; validation, R.R and N.S.F.D; investigation, M.A.D.J.; resources, R.R.; writing original draft preparation, N.S.F.D. and M.A.D.J.; writing review and editing, R.R,

N.A.M.F., A.S.M.K., S.A.M.; visualization, M.A.D.J.; supervision, R.R.; funding acquisition, R.R.

Conflicts of Interest

The authors declare no conflict of interest.

Artificial Intelligence (AI) Transparency Statement

ChatGPT were used only to enhance grammar, clarity, and manuscript readability. They were not used to generate, analyze, or interpret data, nor to create scientific hypotheses, conclusions, or literature reviews. All content remains the intellectual product of the authors. Any AI-assisted text was carefully checked, revised, and validated to ensure compliance with research integrity and publisher guidelines.

References

Abdelmigid, H.M., Hussien, N.A., Alyamani, A.A., Morsi, M.M., AlSufyani, N.M. and Kadi, H.A. (2022) 'Green synthesis of zinc oxide nanoparticles using pomegranate fruit peel and solid coffee grounds vs. chemical method of synthesis, with their biocompatibility and antibacterial properties investigation', *Molecules*, 27(4), p. 1236.

Adjonu, R., Doran, G.S., Torley, P., Sampson, G.O. and Agboola, S.O. (2022) 'Whey protein peptides have dual functions: Bioactivity and emulsifiers in oil-in-water nanoemulsion', *Foods*, 11(12), p. 1812.

Alhaddad, R., Abualsoud, B.M., Al-Deeb, I. and Nsairat, H. (2024) 'Green synthesized Zingiber officinale-ZnO nanoparticles: anticancer efficacy against 3D breast cancer model', *Future Science OA*, 10(1), p. 2419806.

Amirabedi, P., Yegani, R. and Hesaraki, A.H. (2017) 'Hydrophobicity optimization of polypropylene hollow fiber membrane by sol–gel process for CO 2 absorption in gas–liquid membrane contactor using response surface methodology', *Iranian Polymer Journal*, 26, pp. 431–443.

Bakeshlou, H., Pirsa, S., Mohtarami, F. and Bener, M. (2024) 'Investigating the structural and antimicrobial properties of wheat gluten nanocomposite film containing zinc oxide nanoparticles and quercetin nanoliposomes', *Journal of Polymers and the Environment*, 32(10), pp. 4925–4944.

Bayda, S., Adeel, M., Tuccinardi, T., Cordani, M. and Rizzolio, F. (2019) 'The history of nanoscience and nanotechnology: from chemical–physical applications to

nanomedicine', *Molecules*, 25(1), p. 112.

Cadena, D.M., Sowa, J.K., Cotton, D.E., Wight, C.D., Hoffman, C.L., Wagner, H.R., Boette, J.T., Raulerson, E.K., Iverson, B.L. and Rossky, P.J. (2022) 'Aggregation of charge acceptors on nanocrystal surfaces alters rates of photoinduced electron transfer', *Journal of the American Chemical Society*, 144(49), pp. 22676–22688.

Chuo, S.C. and Setapar, S.H.M. (2022) 'Application of nanoemulsion in cosmetics', in *Nanotechnology for the preparation of cosmetics using plant-based extracts*. Elsevier, pp. 355–371.

Dzulkharnien, N.S.F., Rohani, R., Kofli, N.T., Kasim, N.A.M., Muid, S.A., Patrick, M., Fauzi, N.A.M., Alias, H. and Radzuan, H.A. (2024) 'Enhanced binding interaction and antibacterial inhibition for nanometal oxide particles activated with Aloe Vulgarize through one-pot ultrasonication techniques', *Bioorganic Chemistry*, p. 107513.

Hunter, S.J., Chohan, P., Varlas, S. and Armes, S.P. (2024) 'Effect of temperature, oil type, and copolymer concentration on the long-term stability of oil-in-water pickering nanoemulsions prepared using diblock copolymer nanoparticles', *Langmuir*, 40(7), pp. 3702–3714.

Jaiswal, M., Dudhe, R. and P K Sharma (2014) 'an advanced mode of drug delivery system. 3 Biotech. 2015 Apr; 5 (2): 123–127', *Published online* [Preprint].

Kalaba, M.H., El-Sherbiny, G.M., Ewais, E.A., Darwesh, O.M. and Moghannem, S.A. (2024) 'Green synthesis of zinc oxide nanoparticles (ZnO-NPs) by Streptomyces baarnensis and its active metabolite (Ka): a promising combination against multidrug-resistant ESKAPE pathogens and cytotoxicity', *BMC microbiology*, 24(1), p. 254.

Kampa, J., Koidis, A., Ghawi, S.K., Frazier, R.A. and Rodriguez-Garcia, J. (2022) 'Optimisation of the physicochemical stability of extra virgin olive oil-in-water nanoemulsion: processing parameters and stabiliser type', *European Food Research and Technology*, 248(11), pp. 2765–2777.

Kaur, G., Panigrahi, C., Agarwal, S., Khuntia, A. and Sahoo, M. (2024) 'Recent trends and advancements in nanoemulsions: Production methods, functional properties, applications in food sector, safety and toxicological effects', *Food Physics*, 1, p. 100024.

Kung, M.-L., Lin, P.-Y., Hsieh, C.-W., Tai, M.-H., Wu, D.-C., Kuo, C.-H., Hsieh, S.-L., Chen,

H.-T. and Hsieh, S. (2014) 'Bifunctional peppermint oil nanoparticles for antibacterial activity and fluorescence imaging', *ACS Sustainable Chemistry & Engineering*, 2(7), pp. 1769–1775.

Lima, M.A., Carusi, J., Rocha, L. de O., Tonon, R.V., Cunha, R.L. and Rosenthal, A. (2024) 'Physicochemical Characterization, Rheological Properties, and Antimicrobial Activity of Sodium Alginate-Pink Pepper Essential Oil (PPEO) Nanoemulsions', *Foods*, 13(19), p. 3090.

Liu, Q., Gao, Y., Fu, X., Chen, W., Yang, J., Chen, Z., Wang, Z., Zhuansun, X., Feng, J. and Chen, Y. (2021) 'Preparation of peppermint oil nanoemulsions: Investigation of stability, antibacterial mechanism and apoptosis effects', *Colloids and Surfaces B: Biointerfaces*, 201, p. 111626.

Mansoori, G.A. and Soelaiman, T.A.F. (2005) 'Nanotechnology--An introduction for the standards community'.

Milinčić, D.D., Salević-Jelić, A.S., Kostić, A.Ž., Stanojević, S.P., Nedović, V. and Pešić, M.B. (2024) 'Food nanoemulsions: How simulated gastrointestinal digestion models, nanoemulsion, and food matrix properties affect bioaccessibility of encapsulated bioactive compounds', *Critical Reviews in Food Science and Nutrition*, 64(22), pp. 8091–8113.

Motelica, L., Oprea, O.-C., Vasile, B.-S., Ficai, A., Ficai, D., Andronescu, E. and Holban, A.M. (2023) 'Antibacterial activity of solvothermal obtained ZnO nanoparticles with different morphology and photocatalytic activity against a dye mixture: methylene blue, rhodamine B and methyl orange', *International Journal of Molecular Sciences*, 24(6), p. 5677.

Mutlu, N. (2024) 'Incorporating Nigella sativa nanoemulsion into gelatin-guar gum films for enhanced healing of wound infections', *Journal of Health Sciences and Medicine*, 7(2), pp. 146–152.

Omar, A.A.A.-H., Gad, M.F., Abdelhafez, H.M., Ebrahem Mersal, A.T. and Mossa, A.-T.H. (2023) 'Phytochemical study, antioxidant potential and preparation of a clove nanoemulsion loaded with pomegranate peel extract', *Egyptian Journal of Chemistry*, 66(13), pp. 21–37.

Saberi, A.H., Fang, Y. and McClements, D.J. (2014) 'Stabilization of vitamin E-enriched

nanoemulsions: influence of post-homogenization cosurfactant addition', *Journal of agricultural and food chemistry*, 62(7), pp. 1625–1633.

Somala, N., Laosinwattana, C. and Teerarak, M. (2022) 'Formulation process, physical stability and herbicidal activities of Cymbopogon nardus essential oil-based nanoemulsion', *Scientific Reports*, 12(1), p. 10280.

Teng, F., He, M., Xu, J., Chen, F., Wu, C., Wang, Z. and Li, Y. (2020) 'Effect of ultrasonication on the stability and storage of a soy protein isolate-phosphatidylcholine nanoemulsions', *Scientific reports*, 10(1), p. 14010.

Thepwatee, S., Pinket, A. and Rangauthok, S. (2024) 'Strategic Development of Nanoemulsion Bases for Versatile Active Ingredient Incorporation', in *Materials Science Forum*. Trans Tech Publ, pp. 9–16.

Zhang, W., Jiang, H., Rhim, J.-W., Cao, J. and Jiang, W. (2022) 'Effective strategies of sustained release and retention enhancement of essential oils in active food packaging films/coatings', *Food Chemistry*, 367, p. 130671.

Zhu, Y., Zhou, Y., Tian, T., Wang, Zhaoyun, Qi, B., Zhang, X., Liu, J., Li, Y., Jiang, L. and Wang, Zhongjiang (2019) 'In vitro simulated digestion and microstructure of peppermint oil nanoemulsion', *Journal of Oleo Science*, 68(9), pp. 863–871.